Nuclear Science and Techniques (2026) 37:102
https://doi.org/10.1007/s41365-026-01934-1

Probing the collision geometry via two-photon processes in heavy-ion collisions

Jia-Xuan Luo[1] · Xin-Bai Li[1] · Ze-Bo Tang[1] · Xin Wu[1] · Shuai Yang[2] · Wang-Mei Zha[1] · Zhan Zhang[1]

Received: 9 May 2025 / Revised: 31 July 2025 / Accepted: 10 August 2025 / Published online: 24 March 2026

Abstract
The initial collision geometry, including the reaction plane, is crucial for interpreting the collective phenomena in relativistic heavy-ion collisions; however, it remains experimentally inaccessible through conventional measurements. Recent studies have proposed the utilization of photon-induced processes as a direct probe, leveraging the complete linear polarization of emitted photons, whose orientation strongly correlates with the collision geometry. In this study, we employed a QED-based approach to systematically investigate dilepton production via two-photon processes in heavy-ion collisions at RHIC and LHC energies and detector acceptances. Our calculations reveal that dilepton emission exhibits significant sensitivity to the initial collision geometry through both the azimuthal angles of their emission (defined by the relative momentum vector of the two leptons) and the overall momentum orientation of dilepton pairs. These findings highlight the potential of two-photon-generated dileptons as a novel polarization-driven probe for quantifying the initial collision geometry and reducing uncertainties in the characterization of quark–gluon plasma properties.

Keywords Heavy-ion collisions · Collision geometry · Two-photon processes · Collective motion

1 Introduction

The primary objective of relativistic heavy-ion collisions is to create and study quark–gluon plasma (QGP), the deconfined state of strongly interacting matter believed to have existed microseconds after the Big Bang [1–3]. Over decades of experimental and theoretical efforts, the formation of QGP under laboratory conditions has been firmly established, marking a pivotal achievement in high-energy nuclear physics. Current research focuses on characterizing QGP properties, such as its transport coefficients, equation of state, and response to extreme electromagnetic fields, and mapping the phase diagram of quantum chromodynamics (QCD) matter [4–8].

The central focus of these investigations is the probing of collective phenomena in heavy-ion collisions, including anisotropic flow, global spin polarization, and chiral magnetic effects [9–14]. These observables, measured extensively across collision energies and systems (e.g., by the STAR, ALICE, and CMS collaborations), reveal that the QGP behaves as a near-perfect fluid with remarkable vorticity, intense electromagnetic fields, and signatures of chiral symmetry restoration [15, 16]. However, a critical challenge persists: The initial collision geometry (e.g., the reaction plane and participant eccentricity) cannot be directly accessed in experiments [17, 18]. Current methods infer the geometry indirectly via final-state momentum anisotropies, inherently conflating the initial-state properties with medium-induced effects, non-flow correlations, and event-by-event fluctuations [19–21]. This introduces systematic biases that obscure the quantitative links between the QGP properties and initial

This work was supported in part by the National Key Research and Development Program of China (No. 2022YFA1604900), the National Natural Science Foundation of China (NSFC) (Nos. 12175223, 124B2103, and 12005220), Anhui Provincial Natural Science Foundation (No. 2208085J23), and the Youth Innovation Promotion Association of Chinese Academy of Sciences and the Chinese Academy of Sciences (CAS) (No. YSBR-088).

✉ Wang-Mei Zha
first@ustc.edu.cn

1 State Key Laboratory of Particle Detection and Electronics, University of Science and Technology of China, Hefei 230026, China

2 State Key Laboratory of Nuclear Physics and Technology, Institute of Quantum Matter, South China Normal University, Guangzhou 510006, China

conditions, underscoring the need for direct probes of the collision geometry.

Recent advances have proposed photon-induced processes in hadronic heavy-ion collisions (HHICs) as a novel pathway to access the initial geometry [22]. When relativistic nuclei collide, their strong electromagnetic fields generate quasi-real photons with polarization vectors oriented perpendicular to the motion of the colliding nucleus [23–25]. These polarized photons initiate coherent processes through both QED and QCD mechanisms:

- **QED-dominated channels**: Photon–photon fusion into dilepton pairs (e.g., e^+e^- via $\gamma\gamma \to e^+e^-$) [26–29], where the photon's linear polarization dictates angular correlations in the decay products [30–32].
- **QCD-assisted processes**: Coherent photoproduction of vector mesons (e.g., J/ψ) through photon–pomeron interactions, where the polarization transfers to the produced meson [33–37].

The photon polarization direction is geometrically encoded by the initial collision configuration, which enables polarization-based probes of the reaction plane. Pioneering studies have validated this hypothesis. Xiao et al. [38] first predicted quadrupole modulation in the azimuthal angle of dileptons (defined by the relative momentum direction $\vec{p}_+ - \vec{p}_-$) from $\gamma\gamma$ processes, directly reflecting the photon polarization anisotropy. Subsequently, Wu et al. [22] proposed leveraging vector meson photoproduction to reconstruct the reaction plane using polarization-induced decay asymmetries. Recently, STAR measurements of coherently photo-produced J/ψ mesons [39] in HHICs confirmed the alignment between the J/ψ decay anisotropy and the reaction plane, cementing photon polarization as a direct probe of the initial geometry.

In this study, we employed our established QED framework [40–42] to quantify dilepton production in HHICs, focusing on their dual sensitivity to both azimuthal emission angles ($\Delta\phi \propto \phi_{\vec{p}_+-\vec{p}_-}$) and momentum orientation ($\Phi_{\text{pair}} \propto \phi_{\vec{p}_++\vec{p}_-}$) relative to the reaction plane. Unlike prior studies that primarily utilized $\Delta\phi$-dependent observables, we demonstrate for the first time that the dilepton pair's total momentum orientation (Φ_{pair}) exhibits significantly enhanced sensitivity to geometric information. Our calculations at RHIC and LHC energies reveal that the geometric constraints from Φ_{pair} exceed those of $\Delta\phi$-based analyses in precision, while both observables provide orthogonal perspectives on the reaction plane, bypassing the systematic uncertainties inherent to traditional flow analyses. This establishes the QED-calibrated dilepton framework, simultaneously leveraging $\Delta\phi$ and Φ_{pair}, as a multi-dimensional probe for the model-independent extraction of the initial geometry.

2 Methodological framework

The equivalent photon approximation (EPA) provides a computationally efficient framework for calculating the total cross sections in heavy-ion collisions through the convolution of photon fluxes with the elementary $\gamma\gamma \to \ell^+\ell^-$ Breit–Wheeler process [23, 43]:

$$\sigma_{\ell^+\ell^-} = \int \frac{\mathrm{d}\omega_1}{\omega_1}\frac{\mathrm{d}\omega_2}{\omega_2} n(\omega_1)n(\omega_2)\sigma_{\gamma\gamma}(\omega_1,\omega_2), \tag{1}$$

where $n(\omega)$ represents the photon flux density and $\sigma_{\gamma\gamma}$ is the elementary Breit–Wheeler cross section. While the EPA accurately describes integrated cross sections, it becomes progressively inadequate for differential observables owing to its inherent neglect of photon transverse momentum correlations and polarization interference effects between scalar (σ_{s}) and pseudoscalar (σ_{ps}) interaction channels.

To overcome these limitations, we employ a lowest order QED formulation based on the external field approximation. Following Ref. [44], the electromagnetic potentials of colliding nuclei in the Lorentz gauge are

$$\begin{aligned} A^1_\mu(q_1,b) &= -2\pi(Z_1e)\delta(q_1^\nu u_{1\nu})\frac{f_1(-q_1^2)}{q_1^2}u^1_\mu e^{iq_1^\tau b_\tau}, \\ A^2_\mu(q_2,0) &= -2\pi(Z_2e)\delta(q_2^\nu u_{2\nu})\frac{f_2(-q_2^2)}{q_2^2}u^2_\mu, \end{aligned} \tag{2}$$

where $q_{1,2}$ are the equivalent photon four momenta, $u^{(1,2)} = \gamma(1,0,0,\pm\beta) =: \gamma w^{(1,2)}$ are four velocities in the collider frame,γ and β are the Lorentz factor and velocity of colliding nuclei, b is the impact parameter of the collision, and $f(-q^2)$ denotes the nuclear charge form factor obtained via Fourier transform of the charge density distribution. The charge density of a symmetrical nucleus is characterized by the Woods–Saxon profile as follows:

$$\rho(r) = \frac{\rho_0}{1+\exp\left[(r-R_{\text{WS}})/d\right]}, \tag{3}$$

where R_{WS} represents the nuclear radius and d denotes the surface diffuseness parameter, both of which are determined from electron scattering measurements [45, 46]. The normalization constant ρ_0 ensures $\int_0^\infty \rho(r)4\pi r^2\mathrm{d}r = A$.

With the direct and cross Feynman diagrams of the lowest order two-photon interaction for lepton pair creation, the matrix element can be expressed as [47]

$$\mathcal{M} = \bar{u}(p_-)\hat{\mathcal{M}}v(p_+), \tag{4}$$

where

$$\begin{aligned}\hat{\mathcal{M}} =& - ie^2 \int \frac{d^4 q_1}{(2\pi)^4} \not{A}^{(1)}(q_1) \frac{\not{p}_- - \not{q}_1 + m}{(p_- - q_1)^2 - m^2} \not{A}^{(2)}(q_2) \\ &- ie^2 \int \frac{d^4 q_1}{(2\pi)^4} \not{A}^{(2)}(q_2) \frac{\not{q}_1 - \not{p}_+ + m}{(q_1 - p_+)^2 - m^2} \not{A}^{(1)}(q_1) \\ =& - i \left(\frac{Ze^2}{2\pi}\right)^2 \frac{1}{2\beta} \int d^2 q_{1\perp} \frac{1}{q_1^2} \frac{1}{q_2^2} \exp(iq_{1\perp} b) \\ &\times \left\{ \frac{\not{\psi}^{(1)}(\not{p}_- - \not{q}_1 + m)\not{\psi}^{(2)}}{[(p_- - q_1)^2 - m^2]} + \frac{\not{\psi}^{(2)}(\not{q}_1 - \not{p}_+ + m)\not{\psi}^{(1)}}{[(q_1 - p_+)^2 - m^2]} \right\}\end{aligned} \tag{5}$$

with $q_2 \equiv p_+ + p_- - q_1$. The four momenta of the produced leptons are denoted by p_+ and p_-, while the longitudinal components of the quasi-real photon four momenta q_1 are constrained through the relations:

$$q_1^0 = \frac{1}{2}\left[(\varepsilon_+ + \varepsilon_-) + \beta(p_+^z + p_-^z)\right], \tag{6}$$

$$q_1^z = q_1^0/\beta, \tag{7}$$

where $\varepsilon_\pm$ is the lepton energy, and m is the lepton mass. The probability of the lowest order pair production can then be expressed as:

$$\begin{aligned}P(p_+, p_-; b) =& \sum_{\text{spin}} |\mathcal{M}|^2 \\ =& \frac{4}{\beta^2} \int d^2 q_{1\perp}\, d^2 \Delta q_\perp\, e^{i\Delta q_\perp b} \prod_{i=0,1,3,4} f(N_i) F(N_i) \\ &\times \mathrm{Tr} \Bigg\{ (\not{p}_- + m) \Big[N_{2D}^{-1} \not{\psi}_1 (\not{p}_- - \not{q}_1 + m) \not{\psi}_2 \\ &+ N_{2X}^{-1} \not{\psi}_2 (\not{q}_1 - \not{p}_+ + m) \not{\psi}_1 \Big] \\ &\times (\not{p}_+ - m) \Big[N_{5D}^{-1} \not{\psi}_2 (\not{p}_- - \not{q}_1 + \not{\Delta q} + m) \not{\psi}_1 \\ &+ N_{5X}^{-1} \not{\psi}_1 (\not{q}_1 + \not{\Delta q} - \not{p}_+ + m) \not{\psi}_2 \Big] \Bigg\},\end{aligned} \tag{8}$$

with

$$\begin{aligned}N_0 &= -q_1^2, \\ N_1 &= -[q_1 - (p_+ + p_-)]^2, \\ N_3 &= -(q_1 + \Delta q)^2, \\ N_4 &= -[\Delta q + (q_1 - p_+ - p_-)]^2, \\ N_{2D} &= -(q_1 - p_-)^2 + m^2, \\ N_{2X} &= -(q_1 - p_+)^2 + m^2, \\ N_{5D} &= -(q_1 + \Delta q - p_-)^2 + m^2, \\ N_{5X} &= -(q_1 + \Delta q - p_+)^2 + m^2,\end{aligned} \tag{9}$$

where $F(N_i)$ represents the photon propagators that describe the interaction with the Coulomb field of both nuclei [42, 48, 49]:

$$F(k) = 2\pi \int d\rho \rho J_0(k\rho) \left\{ \exp\left[2iZ\alpha K_0(\rho\omega/\gamma)\right] - 1 \right\} \tag{10}$$

and Δq is the four-momentum difference between q_1 and q_1' ($\Delta q \equiv q_1 - q_1'$), with propagator assignments organized as

- $i = \mathbf{0, 3}$ **terms**: originate from nucleus 1 (direct/conjugate photons q_1 and q_1');
- $i = \mathbf{1, 4}$ **terms**: sourced from nucleus 2 (direct/conjugate photons q_2 and q_2').

We construct angular correlations as follows:

$$\Phi_{\text{pair}} \equiv \phi_{\vec{p}_+ + \vec{p}_-} - \phi_b, \tag{11}$$

$$\Delta\phi \equiv \phi_{\vec{p}_+ - \vec{p}_-} - \phi_b, \tag{12}$$

where ϕ_b denotes the azimuthal angle of impact parameter b. The differential distribution $dN/d\Phi_{\text{pair}}$ is obtained by integrating over:

$$\int_{\Omega_{\text{phase}}} \delta(\Phi_{\text{pair}} - f[\vec{p}_\pm, b])\, P(p_+, p_-; b)\, \mathcal{J} d\Omega_{\text{reduce}}, \tag{13}$$

where $f[\vec{p}_\pm, b]$ maps the momentum combinations to the angular differences derived from Eqs. 11 and 12, $\mathcal{J}$ contains the Jacobian factors from the coordinate transformations, and $d\Omega_{\text{reduce}}$ denotes integration over the non-angular momentum components. Similarly, $dN/d(\Delta\phi)$ can be obtained by following the procedure outlined in Eq. 13. High-dimensional phase space integration was performed using the VEGAS adaptive Monte Carlo algorithm [50] within the ROOT framework [51].

Although the QED formulation provides precise calculations of angular correlations, the dynamical mechanism through which photon polarization induces angular asymmetry (with respect to the impact parameter) remains implicit. To unveil the physical origins of this connection, we traced how the field geometry (governing polarization directions) dynamically "locks" onto the momentum-space characteristics of the produced particles. Consider the electromagnetic field configuration in peripheral heavy-ion collisions: Quasi-real photons carry linear polarization determined by classical electromagnetic fields. Specifically, the electric field vector $\vec{\varepsilon}$ at a transverse position $\vec{r}_\perp$ (defined with respect to the nucleus center as the origin) satisfies the radial constraint:

$$\vec{\varepsilon}(\vec{r}_\perp) \parallel \vec{r}_\perp,$$

Table 1 Fiducial cuts implemented in the calculation

Process and beam energy		p_{Tl} (GeV/c)	η_{l}	P_{Tll} (GeV/c)	Y_{ll}	M_{ll} (GeV/c^2)
$\gamma\gamma \to e^+e^-(\mu^+\mu^-)$	Au+Au $\sqrt{s_{\mathrm{NN}}} = 200$ GeV	$(0.2, +\infty)$	$(-1.0, 1.0)$	$(0, 0.1)$	$(-1.0, 1.0)$	$(0.4, 2.6)$
$\gamma\gamma \to e^+e^-$	Pb+Pb $\sqrt{s_{\mathrm{NN}}} = 5.02$ TeV	$(0.5, +\infty)$	$(-1.0, 1.0)$	$(0, 0.1)$	$(-1.0, 1.0)$	$(1.0, 2.8)$
$\gamma\gamma \to \mu^+\mu^-$	Pb+Pb $\sqrt{s_{\mathrm{NN}}} = 5.02$ TeV	$(4.0, +\infty)$	$(-2.4, 2.4)$	$(0, 0.1)$	$(-2.4, 2.4)$	$(8.0, 100.0)$

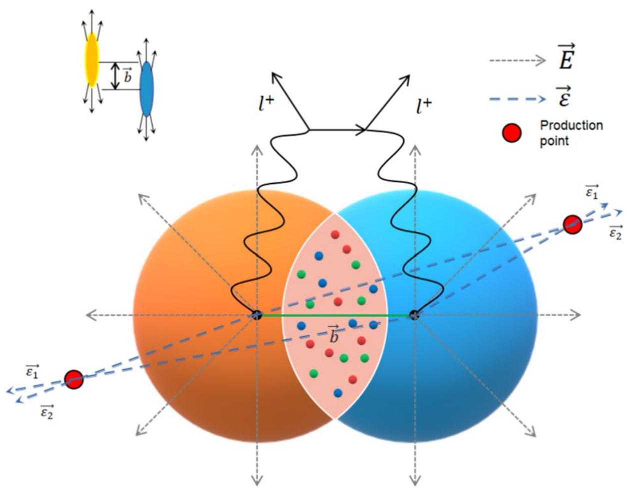

Fig. 1 (Color online) Electromagnetic field configuration in transverse plane with collision impact parameter b

this indicates that the electric field direction is radially oriented away from the nucleus center, as illustrated by the field line distribution in Fig. 1. This spatial polarization pattern becomes imprinted on the photon momentum distribution through the Fourier relation $\vec{q}_\perp \leftrightarrow \vec{r}_\perp$, leading to the momentum-polarization locking

$$\vec{\varepsilon}(\vec{q}_\perp) \parallel \vec{q}_\perp. \tag{14}$$

In the dilepton production process $\gamma\gamma \to \ell^+\ell^-$, the scattering amplitude depends critically on the relative orientation of the photon polarization:

$$\mathcal{M} \propto \left(\vec{\varepsilon}_1 \cdot \vec{\varepsilon}_2\right) \times \text{lepton current}. \tag{15}$$

The polarization overlap $|\vec{\varepsilon}_1 \cdot \vec{\varepsilon}_2|$ reaches maximum when the two photons' transverse momenta are collinear ($\vec{q}_{\perp 1} \parallel \vec{q}_{\perp 2}$). As illustrated in Fig. 1, this collinear condition forces the pair orientation Φ_{pair} to align with the impact parameter. The observed $\Delta\phi$ asymmetry stems from the geometric suppression of the polarization correlations owing to angular misalignment. Specifically, as shown in Fig. 1, when the transverse momenta $\vec{q}_{\perp 1}$ and $\vec{q}_{\perp 2}$ acquire non-collinear components (induced by a finite impact parameter b), their polarization vectors $\vec{\varepsilon}_1$ and $\vec{\varepsilon}_2$ become mismatched. These misalignments introduce a characteristic modulation in the angular distribution, dominated by $\cos(2\Delta\phi)$ and $\cos(4\Delta\phi)$ terms with respect to the impact parameter axis, which are direct consequences of the spin-1 nature of photons and spin-1/2 nature of leptons in the $\gamma\gamma \to$ dilepton production process [25].

3 Results

Figure 2 illustrates the azimuthal modulations of dimuon pairs with respect to the reaction plane in peripheral Au+Au collisions at $\sqrt{s_{\mathrm{NN}}} = 200$ GeV (RHIC) with an impact

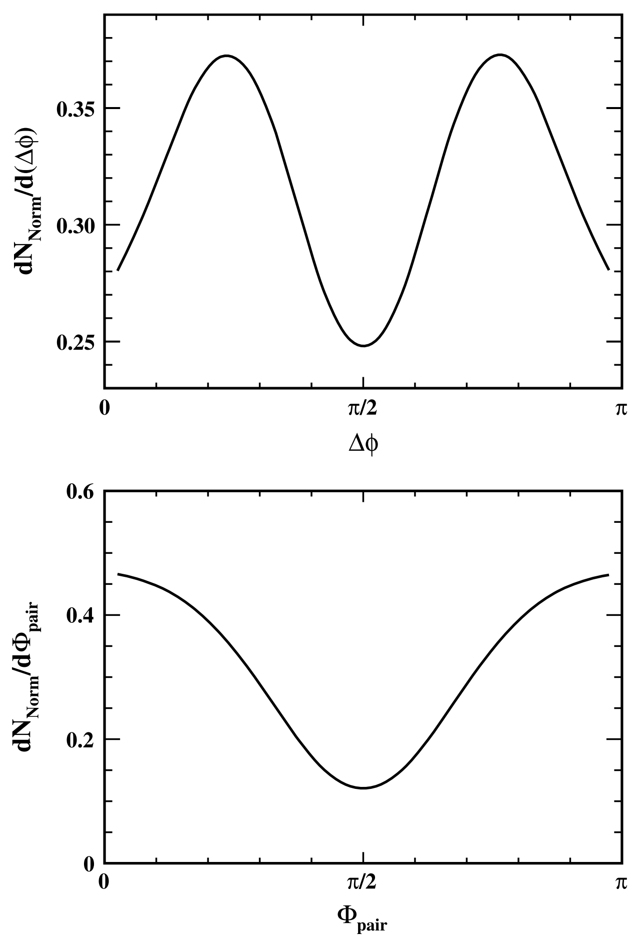

Fig. 2 The periodic oscillation pattern in the alignment of the $\phi_{\vec{p}_+ + \vec{p}_-}$ and $\phi_{\vec{p}_+ - \vec{p}_-}$ related to the reaction plane ϕ_b for the dimuon pair production in Au+Au peripheral collisions at $\sqrt{s_{\mathrm{NN}}} = 200$ GeV with impact parameter $b = 11$ fm

parameter $b = 11$ fm. The detailed fiducial cuts applied in the calculations are presented in Table 1. The $\Delta\phi$ distribution exhibits a dominant $\cos(4\Delta\phi)$ pattern owing to the spin of the interacting photons. A secondary $\cos(2\Delta\phi)$ modulation, originating from lepton mass effects, becomes visible as the finite muon mass breaks the helicity conservation. In contrast, the Φ_{pair} distribution shows a pronounced $\cos(2\Phi_{\text{pair}})$ modulation, which directly reflects the alignment of the dilepton total momentum with the reaction plane. This alignment arises from the momentum-polarization locking effect discussed in Sect. 2, where the global polarization geometry encoded in the electromagnetic fields is imprinted onto the angular correlation of the dilepton pairs.

The invariant mass dependence of anisotropic coefficients $\langle\cos(4\Delta\phi)\rangle$ and $\langle\cos(2\Phi_{\text{pair}})\rangle$ is shown in Fig. 3. At low mass ($M_{\mu\mu} < 0.8\,\text{GeV}/c^2$), the $\langle\cos(2\Delta\phi)\rangle$ component is visible owing to the violation of helicity conservation. This coefficient diminishes as $M_{\mu\mu}$ increases beyond $0.8\,\text{GeV}/c^2$, and is suppressed by the restoration of helicity conservation. The $\langle\cos(4\Delta\phi)\rangle$ coefficient displays a non-monotonic trend, initially decreasing to a local minimum at $M_{\mu\mu} \sim 0.8$ GeV/c^2 before rising again at higher mass. This behavior reflects competing contributions from two physical mechanisms: Geometric depolarization effects dominate at intermediate mass, while polarization coherence strengthens at larger $M_{\mu\mu}$ as dileptons are preferentially produced near the nuclear periphery. In contrast, the $\langle\cos(2\Phi_{\text{pair}})\rangle$ coefficient retains a consistently positive nonzero value and increases monotonically with the dimuon invariant mass. This distinct mass dependence highlights its enhanced sensitivity as a global geometric observable to local kinematic configurations compared to $\langle\cos(4\Delta\phi)\rangle$.

Figure 4 shows the rapidity dependence of these coefficients for $0.4 < M_{\mu\mu} < 2.6$ GeV/c^2. The magnitude of $\langle\cos(4\Delta\phi)\rangle$ increases with $|y|$, driven by the enhanced polarization alignment in the forward/backward regions, where photoproduction occurs closer to the nuclear surfaces. This spatial localization amplifies the correlation between the photon polarization vectors and the impact parameter orientation. However, within the rapidity range $|y| < 0.8$, the $\langle\cos(2\Phi_{\text{pair}})\rangle$ coefficient remains approximately constant and exhibits a negligible rapidity dependence. This distinct behavior arises because the total momentum orientation of dilepton pairs depends primarily on the vector sum of photon momenta, which is a global property governed by the reaction plane geometry rather than local rapidity-dependent dynamics.

The impact parameter dependence of the modulation coefficients calculated for both the RHIC and LHC collision systems is presented in Fig. 5. Central collisions ($b \to 0$) yield vanishing anisotropies as the polarization geometry becomes azimuthally asymmetrical. The magnitudes of the coefficients grow with increasing b, reaching maxima near $b \sim 2R_A$ (R_A is the nuclear radius). Beyond this point, $\langle\cos(4\Delta\phi)\rangle$ and $\langle\cos(2\Phi_{\text{pair}})\rangle$ stabilize and slightly decrease owing to the depletion of photon flux coherence at ultra-peripheral separations. The impact parameter dependence of $\langle\cos(4\Delta\phi)\rangle$ behaves similarly to Xiao's calculations [38], despite the distinct pair p_{T} ranges. Remarkably, the $\langle\cos(2\Phi_{\text{pair}})\rangle$ values consistently exceed those of $\langle\cos(4\Delta\phi)\rangle$ across the entire b range, demonstrating the superior sensitivity of pair momentum orientation to collision geometry. This systematic trend persists in Pb+Pb collisions at $\sqrt{s_{\text{NN}}} = 5.02$ TeV (LHC),

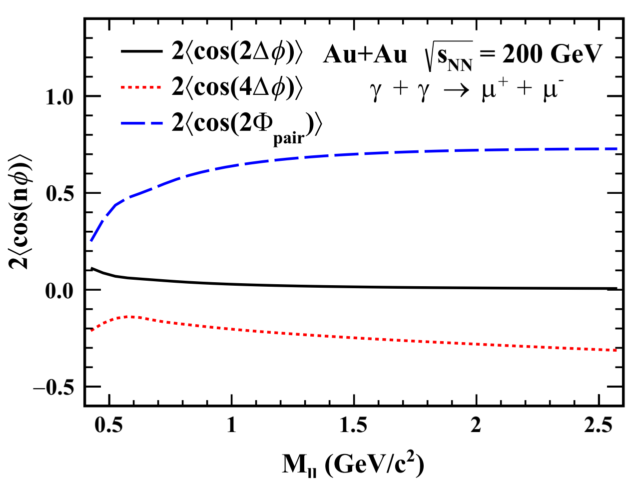

Fig. 3 Second- and fourth-order modulation coefficients $2\langle\cos(n\phi)\rangle$ for $\Delta\phi$ and Φ_{pair} as a function of dimuon invariant mass in Au+Au peripheral collisions at $\sqrt{s_{\text{NN}}} = 200$ GeV with impact parameter $b = 11$ fm

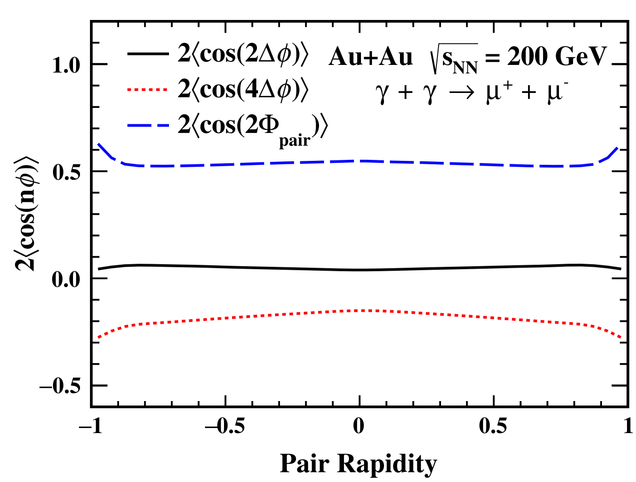

Fig. 4 Second- and fourth-order modulation coefficients $2\langle\cos(n\phi)\rangle$ for $\Delta\phi$ and Φ_{pair} as a function of dimuon pair rapidity in Au+Au peripheral collisions at $\sqrt{s_{\text{NN}}} = 200$ GeV with impact parameter $b = 11$ fm

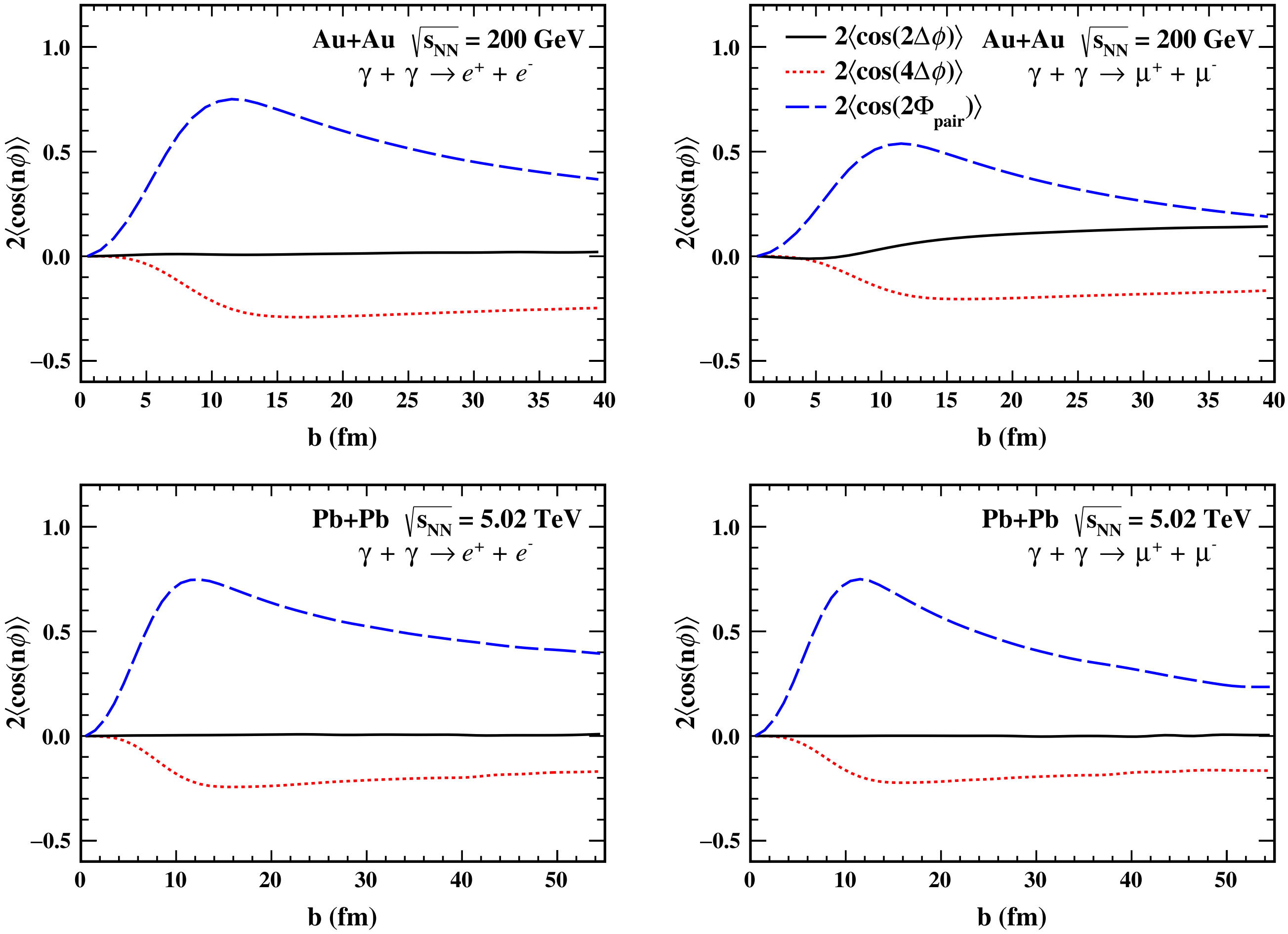

Fig. 5 Second- and fourth-order modulation coefficients $2\langle\cos(n\phi)\rangle$ for $\Delta\phi$ and Φ_{pair} as a function of impact parameter in Au+Au collisions at $\sqrt{s_{\text{NN}}}$ = 200 GeV (RHIC) and Pb+Pb collisions at $\sqrt{s_{\text{NN}}}$ = 5.02 TeV (LHC)

confirming the universality of QED-dominated polarization effects across various collision energies.

Collectively, these results establish Φ_{pair} correlations as a precision tool for the initial geometry determination. The distinct dependence of $\langle\cos(2\Phi_{\text{pair}})\rangle$ on mass and rapidity can effectively mitigate the systematic bias induced by final-state interactions, while its strong b-dependence enables direct mapping between observable angular modulations and collision geometry. Complementary information from $\Delta\phi$ harmonics provides cross-checks on polarization purity, which is crucial for separating two-photon processes from competing hadronic backgrounds. The combined analysis of both observables opens a new pathway for the model-independent extraction of the reaction plane in heavy-ion collisions, free from assumptions about medium evolution or hadronization dynamics.

4 Summary

In summary, we employed a QED-based approach to systematically investigate how photon-induced processes can constrain the initial collision geometry in heavy-ion collisions at RHIC and LHC energies. This work introduces a novel observable, the total momentum orientation of the dilepton pair Φ_{pair}, which demonstrates significantly enhanced sensitivity to geometric features, exceeding $\Delta\phi$-based analyses in precision. By combining the complementary sensitivities of the photo-produced dilepton to primordial geometry via both $\Delta\phi$ and Φ_{pair}, our calculations establish the QED-calibrated dilepton framework as a robust, multi-dimensional probe that enables model-independent reconstruction of the collision geometry, offers orthogonal constraints on reaction plane determination, and bypasses systematic uncertainties inherent to traditional flow methods. Future measurements of these observables are expected to provide direct and unambiguous experimental constraints on primordial geometry in relativistic heavy-ion collisions.

Author Contributions All authors contributed to the study conception and design. Material preparation, data collection, and analysis were performed by Jia-Xuan Luo, Xin-Bai Li, and Wang-Mei Zha. The first draft of the manuscript was written by Jia-Xuan Luo, and all authors commented on previous versions of the manuscript. All authors read and approved the final manuscript.

Data Availability The data that support the findings of this study are openly available in Science Data Bank at https://cstr.cn/31253.11.sciencedb.j00186.00972 and https://doi.org/10.57760/sciencedb.j00186.00972.

Declarations

Conflict of interest The authors declare that they have no conflict of interest.

References

1. P. Braun-Munzinger, J. Stachel, The quest for the quark-gluon plasma. Nature **448**, 302–309 (2007). https://doi.org/10.1038/nature06080
2. J. Adams, M.M. Aggarwal, Z. Ahammed et al., Experimental and theoretical challenges in the search for the quark gluon plasma: The STAR Collaboration's critical assessment of the evidence from RHIC collisions. Nucl. Phys. A **757**, 102–183 (2005). https://doi.org/10.1016/j.nuclphysa.2005.03.085
3. Y. Aoki, G. Endrodi, Z. Fodor et al., The Order of the quantum chromodynamics transition predicted by the standard model of particle physics. Nature **443**, 675–678 (2006). https://doi.org/10.1038/nature05120
4. H.T. Ding, F. Karsch, S. Mukherjee, Thermodynamics of strong-interaction matter from Lattice QCD. Int. J. Mod. Phys. E **24**(10), 1530007 (2015). https://doi.org/10.1142/S0218301315300076
5. H. Stoecker, Collective flow signals the quark gluon plasma. Nucl. Phys. A **750**, 121–147 (2005). https://doi.org/10.1016/j.nuclphysa.2004.12.074
6. C.H. Zhang, Q.C. Feng, Y.Y. Ren et al., Magnetic field evolution in Au+Au collisions at $\sqrt{s_{\rm NN}}$ = 200 GeV. Sci. Rep. **13**(1), 21500 (2023). https://doi.org/10.1038/s41598-023-48705-1
7. K. Fukushima, T. Hatsuda, The phase diagram of dense QCD. Rept. Prog. Phys. **74**, 014001 (2011). https://doi.org/10.1088/0034-4885/74/1/014001
8. Y. Zhang, D. Zhang, X.F. Luo, Experimental study of the QCD phase diagram in relativistic heavy-ion collisions. Nucl. Tech. (in Chinese) **46**(04), 040001 (2023). https://doi.org/10.11889/j.0253-3219.2023.hjs.46.040001
9. J. Adams, M.M. Aggarwal, Z. Ahammed et al., Azimuthal anisotropy in Au+Au collisions at $\sqrt{s_{\rm NN}}$ = 200-GeV. Phys. Rev. C **72**, 014904 (2005). https://doi.org/10.1103/PhysRevC.72.014904
10. D.E. Kharzeev, J. Liao, S.A. Voloshin et al., Chiral magnetic and vortical effects in high-energy nuclear collisions—A status report. Prog. Part. Nucl. Phys. **88**, 1–28 (2016). https://doi.org/10.1016/j.ppnp.2016.01.001
11. Z.T. Liang, X.N. Wang, Globally polarized quark-gluon plasma in non-central A+A collisions. Phys. Rev. Lett. **94**, 102301 (2005). https://doi.org/10.1103/PhysRevLett.94.102301
12. M. Abdallah, B.E. Aboona, J. Adam et al., Search for the chiral magnetic effect with isobar collisions at $\sqrt{s_{NN}}$=200 GeV by the STAR Collaboration at the BNL Relativistic Heavy Ion Collider. Phys. Rev. C **105**, 014901 (2022). https://doi.org/10.1103/PhysRevC.105.014901
13. D.P. Anderle, V. Bertone, X. Cao et al., Electron-ion collider in China. Front. Phys. (Beijing) **16**(6), 64701 (2021). https://doi.org/10.1007/s11467-021-1062-0
14. J.H. Chen, Z.T. Liang, Y.G. Ma et al., Vector meson's spin alignments in high energy reactions. Sci. China Phys. Mech. Astron. **68**(1), 211001 (2025). https://doi.org/10.1007/s11433-024-2495-1
15. J.E. Bernhard, J.S. Moreland, S.A. Bass, Bayesian estimation of the specific shear and bulk viscosity of quark–gluon plasma. Nature Phys. **15**(11), 1113–1117 (2019). https://doi.org/10.1038/s41567-019-0611-8
16. F. Becattini, M.A. Lisa, Polarization and vorticity in the Quark-Gluon Plasma. Ann. Rev. Nucl. Part. Sci. **70**, 395–423 (2020). https://doi.org/10.1146/annurev-nucl-021920-095245
17. M.L. Miller, K. Reygers, S.J. Sanders et al., Glauber modeling in high energy nuclear collisions. Ann. Rev. Nucl. Part. Sci. **57**, 205–243 (2007). https://doi.org/10.1146/annurev.nucl.57.090506.123020
18. J. Jia, G. Giacalone, B. Bally et al., Imaging the initial condition of heavy-ion collisions and nuclear structure across the nuclide chart. Nucl. Sci. Tech. **35**, 220 (2024). https://doi.org/10.1007/s41365-024-01589-w
19. G.Y. Qin, H. Petersen, S.A. Bass et al., Translation of collision geometry fluctuations into momentum anisotropies in relativistic heavy-ion collisions. Phys. Rev. C **82**, 064903 (2010). https://doi.org/10.1103/PhysRevC.82.064903
20. B. Alver, B.B. Back, M.D. Baker et al., Non-flow correlations and elliptic flow fluctuations in gold-gold collisions at $\sqrt{s_{\rm NN}}$ = 200 GeV. Phys. Rev. C **81**, 034915 (2010). https://doi.org/10.1103/PhysRevC.81.034915
21. J. Jia, Event-shape fluctuations and flow correlations in ultra-relativistic heavy-ion collisions. J. Phys. G **41**(12), 124003 (2014). https://doi.org/10.1088/0954-3899/41/12/124003
22. X. Wu, X. Li, Z. Tang et al., Reaction plane alignment with linearly polarized photon in heavy-ion collisions. Phys. Rev. Res. **4**(4), L042048 (2022). https://doi.org/10.1103/PhysRevResearch.4.L042048
23. F. Krauss, M. Greiner, G. Soff, Photon and gluon induced processes in relativistic heavy ion collisions. Prog. Part. Nucl. Phys. **39**, 503–564 (1997). https://doi.org/10.1016/S0146-6410(97)00049-5
24. C. Li, J. Zhou, Y.J. Zhou, Probing the linear polarization of photons in ultraperipheral heavy ion collisions. Phys. Lett. B **795**, 576–580 (2019). https://doi.org/10.1016/j.physletb.2019.07.005
25. J. Adam, L. Adamczyk, J.R. Adams et al., Measurement of e^+e^- momentum and angular distributions from linearly polarized photon collisions. Phys. Rev. Lett. **127**(5), 052302 (2021). https://doi.org/10.1103/PhysRevLett.127.052302
26. J. Adam, L. Adamczyk, J.R. Adams et al., Low-$p_{\rm T}$ e^+e^- pair production in Au+Au collisions at $\sqrt{s_{NN}}$ = 200 GeV and U+U collisions at $\sqrt{s_{NN}}$ = 193 GeV at STAR. Phys. Rev. Lett. **121**(13), 132301 (2018). https://doi.org/10.1103/PhysRevLett.121.132301
27. M. Aaboud, et al. (ATLAS), Observation of centrality-dependent acoplanarity for muon pairs produced via two-photon scattering in Pb+Pb collisions at $\sqrt{s_{\rm NN}}$ = 5.02 TeV with the ATLAS

detector. Phys. Rev. Lett. 121(21), 212301 (2018). https://doi.org/10.1103/PhysRevLett.121.212301
28. W. Zha, L. Ruan, Z. Tang et al., Coherent lepton pair production in hadronic heavy ion collisions. Phys. Lett. B **781**, 182–186 (2018). https://doi.org/10.1016/j.physletb.2018.04.006
29. H.S. Shao, D. d'Enterria, gamma-UPC: automated generation of exclusive photon-photon processes in ultraperipheral proton and nuclear collisions with varying form factors. JHEP **09**, 248 (2022). https://doi.org/10.1007/JHEP09(2022)248
30. S. Klein, P. Steinberg, Photonuclear and two-photon Interactions at high-energy nuclear colliders. Ann. Rev. Nucl. Part. Sci. **70**, 323–354 (2020). https://doi.org/10.1146/annurev-nucl-030320-033923
31. J.D. Brandenburg, J. Seger, Z. Xu et al., Report on progress in physics: observation of the Breit-Wheeler process and vacuum birefringence in heavy-ion collisions. Rept. Prog. Phys. **86**(8), 083901 (2023). https://doi.org/10.1088/1361-6633/acdae4
32. D. Shao, B. Yan, S.R. Yuan et al., Spin asymmetry and dipole moments in τ-pair production with ultraperipheral heavy ion collisions. Sci. China Phys. Mech. Astron. **67**(8), 281062 (2024). https://doi.org/10.1007/s11433-024-2389-y
33. J. Adam, L. Adamczyk, J. R. Adams et al., Observation of excess J/ψ yield at very low transverse momenta in Au+Au collisions at $\sqrt{s_{\mathrm{NN}}} = 200$ GeV and U+U collisions at $\sqrt{s_{\mathrm{NN}}} = 193$ GeV. Phys. Rev. Lett. **123**(13), 132302 (2019). https://doi.org/10.1103/PhysRevLett.123.132302
34. W. Zha, J.D. Brandenburg, L. Ruan et al., Exploring the double-slit interference with linearly polarized photons. Phys. Rev. D **103**(3), 033007 (2021). https://doi.org/10.1103/PhysRevD.103.033007
35. K. Shen, X. Wu, Z. Tang et al., Exploring the photoproduction of ρ and ϕ in hadronic heavy-ion collisions. Eur. Phys. J. C **84**(11), 1167 (2024). https://doi.org/10.1140/epjc/s10052-024-13503-0
36. X. Wu, X. Li, Z. Tang et al., Centrality manipulation in exclusive photoproduction at the Electron-Ion Collider. arXiv:2410.06676 (2024). https://doi.org/10.48550/arXiv.2410.06676
37. X. Wu, X.B. Li, Z.B. Tang et al., Impact parameter manipulation in exclusive photoproduction in Electron-Ion Collisions. Nucl. Sci. Tech. **36**(9), 157 (2025). https://doi.org/10.1007/s41365-025-01704-5
38. B.W. Xiao, F. Yuan, J. Zhou, Momentum anisotropy of leptons from two photon processes in heavy ion collisions. Phys. Rev. Lett. **125**(23), 232301 (2020). https://doi.org/10.1103/PhysRevLett.125.232301
39. K. Wang (STAR), Measurements of photon-induced J/ψ azimuthal anisotropy in isobar collisions at STAR, in 12th International Conference on Hard and Electromagnetic Probes of High-Energy Nuclear Collisions (2024)
40. W. Zha, J.D. Brandenburg, Z. Tang et al., Initial transverse-momentum broadening of Breit-Wheeler process in relativistic heavy-ion collisions. Phys. Lett. B **800**, 135089 (2020). https://doi.org/10.1016/j.physletb.2019.135089
41. W. Zha, Z. Tang, Discovery of higher-order quantum electrodynamics effect for the vacuum pair production. JHEP **08**, 083 (2021). https://doi.org/10.1007/JHEP08(2021)083
42. X. Li, J. Luo, Z. Tang et al., Exploring the higher-order QED effects on the differential distributions of vacuum pair production in relativistic heavy-ion collisions. Phys. Lett. B **847**, 138314 (2023). https://doi.org/10.1016/j.physletb.2023.138314
43. S.R. Klein, J. Nystrand, J. Seger et al., STARlight: A Monte Carlo simulation program for ultra-peripheral collisions of relativistic ions. Comput. Phys. Commun. **212**, 258–268 (2017). https://doi.org/10.1016/j.cpc.2016.10.016
44. M. Vidovic, M. Greiner, C. Best et al, Impact parameter dependence of the electromagnetic particle production in ultrarelativistic heavy ion collisions. Phys. Rev. C **47**, 2308–2319 (1993). https://doi.org/10.1103/PhysRevC.47.2308
45. C.W. De Jager, H. De Vries, C. De Vries, Nuclear charge and magnetization density distribution parameters from elastic electron scattering. Atom. Data Nucl. Data Tabl. **14**, 479–508 (1974). https://doi.org/10.1016/S0092-640X(74)80002-1
46. H. De Vries, C.W. De Jager, C. De Vries, Nuclear charge and magnetization density distribution parameters from elastic electron scattering. Atom. Data Nucl. Data Tabl. **36**, 495–536 (1987). https://doi.org/10.1016/0092-640X(87)90013-1
47. K. Hencken, D. Trautmann, G. Baur, Impact parameter dependence of the total probability for the electromagnetic electron - positron pair production in relativistic heavy ion collisions. Phys. Rev. A **51**, 1874–1882 (1995). https://doi.org/10.1103/PhysRevA.51.1874
48. R.N. Lee, A.I. Milstein, Coulomb corrections to the e+ e- pair production in ultrarelativistic heavy-ion collisions. Phys. Rev. A **61**, 032103 (2000). https://doi.org/10.1103/PhysRevA.61.032103
49. R.N. Lee, A.I. Milstein, Coulomb corrections and multiple e^+e^- pair production in ultrarelativistic nuclear collisions. Phys. Rev. A **64**, 032106 (2001). https://doi.org/10.1103/PhysRevA.64.032106
50. G.P. Lepage, A new algorithm for adaptive multidimensional integration. J. Comput. Phys. **27**, 192 (1978). https://doi.org/10.1016/0021-9991(78)90004-9
51. I. Antcheva, M. Ballintijn, B. Bellenot et al., ROOT: A C++ framework for petabyte data storage, statistical analysis and visualization. Comput. Phys. Commun. **180**, 2499–2512 (2009). https://doi.org/10.1016/j.cpc.2009.08.005